Volume 9 | Number 16 | 21 August 2025

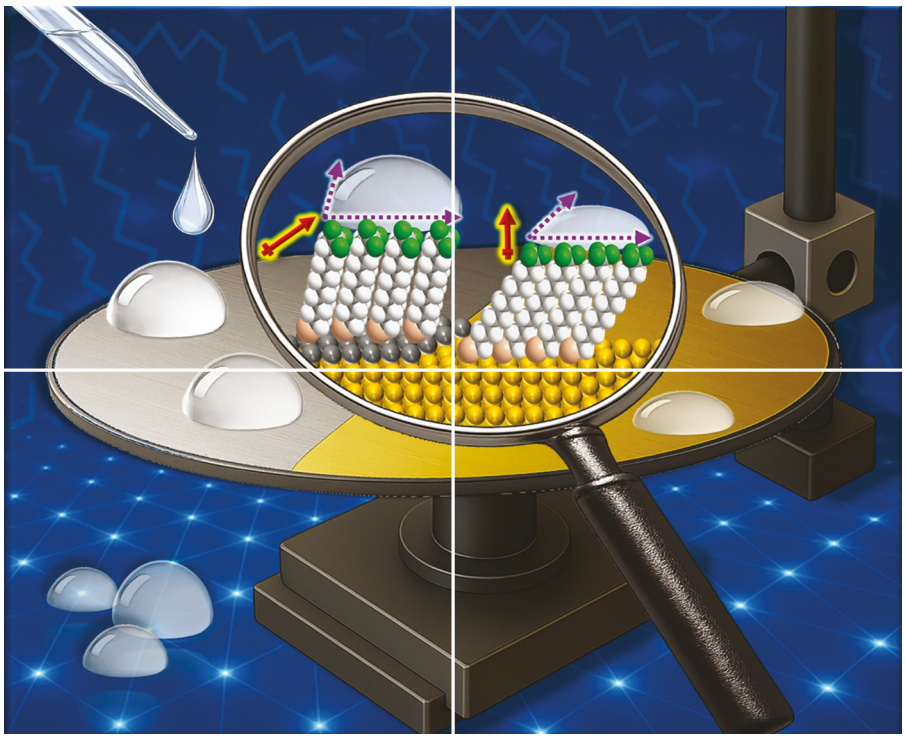

MATERIALS CHEMISTRY

FRONTIERS

CCS 中国化学会 CHINESE CHEMICAL SOCIETY
ICCAS 1956
ROYAL SOCIETY OF CHEMISTRY
rsc.li/frontiers-materials

MATERIALS CHEMISTRY FRONTIERS

CHINESE CHEMICAL SOCIETY

ROYAL SOCIETY OF CHEMISTRY

RESEARCH ARTICLE

View Article Online
View Journal | View Issue

Cite this: *Mater. Chem. Front.*, 2025, **9**, 2478

Underpotentially-deposited silver substrates reverse the odd–even interfacial properties of CF_3-terminated SAMs†

Maria D. Marquez, Ruwanthi Amarasekara, Daniela Rodriguez, Oussama Zenasni, Han Ju Lee, Tianlang Yu, Siwakorn Sakunkaewkasem, Steven Baldelli and T. Randall Lee *

Modifications to the metal substrate used in alkanethiol self-assembled monolayer (SAM) formation impact the structural characteristics of the thin films and their macroscopic interfacial properties. In this study, evaporated gold surfaces underwent electrochemical modification, where a monolayer of silver was deposited through underpotential deposition (UPD). The effects of such a modification of the gold substrate on the structural and interfacial properties of *n*-alkanethiol and CF_3-terminated SAMs, wherein the latter bears an interfacial dipole at the CF_3–CH_2 transition, were explored. Structural analysis of the films revealed well-ordered monolayers on both gold and UPD Ag surfaces. Ellipsometric thickness assessment and X-ray photoelectron spectroscopy (XPS) of UPD Ag surfaces showed that the adsorbates formed densely packed monolayers that were ~4 Å thicker than their counterparts on gold. These variations were attributed to the different binding geometries adopted by the sulfur atoms on the respective metals, which in turn dictates the tilt angles and the orientation of the terminal moiety. Polarization modulation infrared reflection–absorption spectroscopy (PM-IRRAS) revealed a shift in the orientation of the chain termini, likely due to differences in the mobility of underlying methylene units between substrates. Moreover, odd–even effects in the contact angle data of both polar and nonpolar liquids show changes in interfacial wettability further highlighting the impact of the subtle change to the substrate on the film structure.

Received 24th January 2025,
Accepted 16th May 2025

DOI: 10.1039/d4qm00541d

rsc.li/frontiers-materials

Introduction

The ability to tailor the properties of metal surfaces in a controlled manner at the nanoscale is of paramount importance to material engineers and surface scientists. Among the methods developed to achieve such control is the use of self-assembled monolayers (SAMs). In particular, SAMs have seen vast usage in a variety of applications ranging from surfaces pertinent to biological applications,[1,2] lubricants for microelectromechanical systems (MEMs),[3,4] corrosion inhibitors,[5,6] nanoparticle protectants/stabilizers,[7,8] antiadhesive films for surfaces,[9,10] and catalyst modifiers in hydrogenation reactions due to its simplicity to develop the monolayer thin film.[11,12] Among the several types of SAMs, perhaps the most studied systems involve the use of alkanethiols on noble metals, with gold being the most widely used metal. This system continues to be widely studied due to ease of preparation of the films, inertness of the Au substrate, strong Au–S bond of ~50 kcal mol^{-1}, well defined structural features, and the ability to manipulate the interfacial properties of the films *via* synthetic tailoring of the organic adsorbates.[13,14] SAMs generated from thiol adsorbates as well as other headgroups (*i.e.*, carboxylic acids and phosphonic acids) have also been generated on Ag[15] as well as Cu surfaces.[16,17] However, the rapid oxidation of the aforementioned substrates in air make it difficult to work with alkanethiol-based SAM systems.[13]

Consequently, investigating custom metal substrates, where either a SAM deposited substrate or a bare substrate is adorned with a foreign metal species, has been undertaken as an alternative approach to broaden the application of easily oxidizable metals (*i.e.*, silver and copper).[18,19] Such substrates are obtained *via* the electrochemical deposition of the metal species, such as Cd^{2+},[20,21] Pb^{2+},[21–23] Ag^{+},[24,25] and Cu^{2+},[26,27] at a potential less negative than the equilibrium (Nernst) potential for the bulk deposition of the metal.[28,29] The aforementioned phenomenon, known as underpotential deposition (UPD), is dictated by a stronger adatom–substrate interaction than an adatom–adatom

Department of Chemistry and the Texas Center for Superconductivity, University of Houston, Houston, Texas 77204-5003, USA. E-mail: trlee@uh.edu

† Electronic supplementary information (ESI) available. See DOI: https://doi.org/10.1039/d4qm00541d

interaction, which occurs during bulk material deposition, leading to strong adsorption to the dissimilar metal.[30] The UPD of metals has emerged as a method for designing and precisely controlling metal surfaces due to the reproducible control of the surface coverage.[29] The use of UPD has led to understanding nucleation and growth mechanisms of film deposition,[31] measuring the electroactive surface area of metal-based materials,[32] the development of fuel cells *via* the oxidation of glucose,[33] and catalyst preparation.[34] The use of SAMs developed atop UPD metals are limited but has been explored for the enhancement of thermal stability of SAMs on Au,[35–37] the use of non-sulfur adsorbates on Au,[38,39] the post modification of SAM surfaces,[40] as well as SAM templating.[41] Furthermore, the aforementioned studies found that the structural and interfacial properties of the SAMs on UPD Ag differ from those of SAMs on bare Au. Specifically, the observed differences can be attributed to the adlayer structure the SAMs of alkanethiols adopt on the metal surfaces, $(\sqrt{3} \times \sqrt{3})R30^\circ$ on Au(111)[14,15] and $(\sqrt{7} \times \sqrt{7})R19^\circ$ on bulk Ag.[13,42] Thus, our aim is to exploit this inherent difference in adopted structure of the alkanethiols on the metals to tune the interfacial properties of SAM-functionalized surfaces, specifically oriented dipoles.

The ability to tune surface and interfacial properties by generating an array of oriented dipoles on thin films is of significant interest in modern nanotechnology.[43–45] Such surfaces are used in aligning energy levels to achieve work-function modifications in organic field transistors[46,47] and solar cells,[48,49] generating surfaces for the immobilization of biomolecules and biolabeling applications,[50,51] and patterning for photo-responsive surfaces.[52,53] The plethora of SAM-related literature points toward the properties of the generated SAMs as being dictated by the functionality of the organic molecules adsorbed on the surface.[54–56] Altering the distribution of electron density of a film has proven an effective strategy since the order of magnitude and direction of the generated dipole has a profound effect on the interfacial properties of the generated films.[44] In SAMs, interfacial dipoles can be generated by modification of the organic constituent *via* the introduction of electron withdrawing moieties, more specifically highly electronegative fluorine atoms.[57–59] Numerous reports have shown that SAMs generated from selectively fluorinated adsorbates (FSAMs) exhibit extraordinary interfacial properties in the resulting films.[10,60,61] Further, targeting different degrees of fluorination in the terminus of the adsorbate allows for tuning the interfacial properties (*i.e.*, wettability, friction, and adhesion). For instance, minimal fluorination in an alkanethiol (*i.e.*, CF_3-terminated) led to the first example of a class of SAMs with oriented dipoles at the fluorocarbon–hydrocarbon junction (FC–HC), which gave monolayer thin films with a more hydrophilic nature than corresponding alkanethiol films.[62–64] Upon increasing the amount of fluorination in the adsorbate, the influence of the FC–HC dipole diminishes, leading to surfaces that exhibit interfacial properties resembling those of polytetrafluoroethylene.[59,62,65] Further research led to the development of FSAMs with an inverted dipole (*i.e.*, HC–FC representing the hydrocarbon–fluorocarbon junction) as well as alkyl-terminated FSAMs where the HC–FC dipole is systematically buried.[66,67] The impact of the former study lies in the wetting behavior that is governed by the interactions between the interfacial dipole and restrained H-bonded liquids, as highlighted by a reversal in the wettability of the HC–FC-terminated films from the FC–HC-terminated films when in contact with polar protic liquids.[67] The latter study highlights the role both the HC–FC dipole as well as the structure of the adsorbate play on the interfacial properties of the film. To further manipulate surface properties *via* oriented dipoles, herein, we aim to modify evaporated Au substrates by the underpotential deposition of Ag metal in efforts to manipulate the interfacial energetics of monolayers using a series of CF_3-terminated alkanethiols of the form $CF_3(CH_2)_mSH$ (**F1H*m*SH**), where m = 16–19, shown in Fig. 1. Our goal is to not only modulate the FC–HC dipole but also elucidate the effect the UPD Ag plays on the structural properties of the films. As a comparison, the analogous alkanethiols, $CH_3(CH_2)_nSH$ (**H*n*SH**), where n = 18–20, were included in the study.

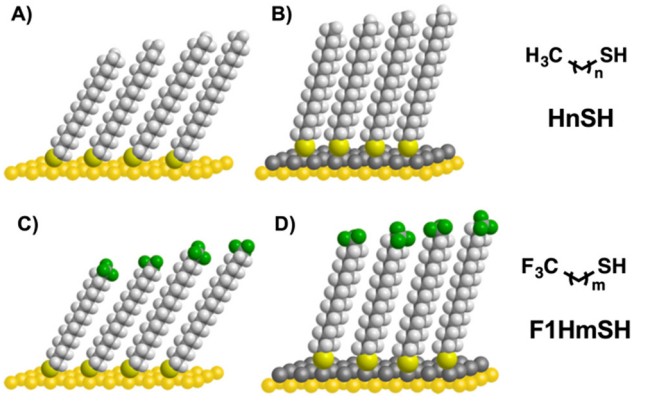

Fig. 1 Molecules used in this study along with an illustration showing the SAMs on Au (A) and (C) and UPD Ag (B) and (D). Hydrogen atoms are denoted as white spheres while fluorine atoms are green.

All SAMs were characterized by ellipsometry to determine the thickness of the films and X-ray photoelectron spectroscopy (XPS) to determine the chemical composition of the films. Polarization-modulation infrared reflection–absorption spectroscopy (PM-IRRAS) was used to determine the conformational order of the films. Finally, contact angle goniometry was used to probe the differences in the wetting properties of the molecules on the different metal substrates.

Experimental

Materials and methods

Gold Shot (99.999%) was bought from Kamis Inc. Chromium rods (99.9%) were purchased from R. D. Mathis Company. Silicon(100) wafers (polished, single crystal) were bought from University Wafer and used as received. Tetrahydrofuran (Sigma-Aldrich) and ethanol (Aaper Alcohol and Chemical Co) used on the SAMs were used as received. The adsorbate 1-octadecanethiol (**H18SH**) was purchased from Sigma-Aldrich. 1-heptadecanethiol

(**H17SH**), 1-nonadecanethiol (**H19SH**), 1-eicosanethiol (**H20SH**), 17,17,17-trifluoroheptadecane-1-thiol (**F1H16SH**), 18,18,18-trifluorooctadecane-1-thiol (**F1H17SH**), 19,19,19-trifluorononadecane-1-thiol (**F1H18SH**), and 20,20,20-trifluoroicosane-1-thiol (**F1H19SH**) were synthesized according to procedures found in the literature.[67,68]

Substrate preparation

Gold slides were prepared by the thermal evaporation of 1000 Å of gold atop 100 Å of chromium on Si(100) wafers under vacuum (pressure $\leq 6 \times 10^{-5}$ torr) at a rate of 0.5 Å s^{-1}. The wafers were then cut into slides and stored in milliQ water until used for electrochemical measurements.

Underpotential deposition of silver (UPD Ag)

For cyclic voltammetry (CV), a Princeton Applied Research potentiostat/galvanostat model 263A was used to modulate the potential applied to and measure the current of the electrochemical systems. A homemade glass cell contained the three electrodes used for electrochemical measurements using gold slides as the working electrodes, a platinum wire as the counter electrode, and mercury/mercurous sulfate in saturated K_2SO_4 as the reference electrode. The reference electrode is +0.64 V relative to the normal hydrogen electrode (NHE). The electrolyte for all CVs was 0.1 M sulfuric acid (Ultrex II Ultrapure Reagent from J. T. Baker) with 0.6 mM Ag_2SO_4 (99.999% trace metals basis from Aldrich) added for the silver voltammetry. Gold slides were cycled ten times in sulfuric acid, rinsed with plenty of milliQ water and stored in milliQ water until measurement of their optical properties with ellipsometry. For the deposition of silver, the cycled gold slides were cycled in deaerated silver solution ten times at a scan rate of 15 mV s^{-1}, then held at a potential of 0.15 V vs MSE for the underpotential deposition of silver,[69] pulled out of the cell while held at potential, rinsed with copious amounts of milliQ water, and stored in milliQ water until analysis with ellipsometry. Representative cyclic voltammograms for gold and silver are shown in Fig. S1 in the ESI.† Using stripping voltammetry, we were able to determine that we have a 0.46 ± 0.03 monolayer coverage of silver on gold. This value was compared to the 0.81 ± 0.04 monolayer value derived from XPS calculations[36] that include silver oxides in the final coverage. A detailed discussion regarding monolayer coverage of Ag and representative voltammograms (Fig. S2, ESI†) are included in the ESI.†

Monolayer formation and characterization

To minimize exposure to the lab environment, immediately after collecting ellipsometric measurements on the bare substrates, the slides were immersed in a 1 mM ethanol solution of the corresponding thiol in a 40 mL vial, previously cleaned with piranha. The self-assembled monolayers were allowed to form for 48 h in the dark at ambient temperature. During this equilibration time, factors such as the high affinity of thiols to Au and Ag substrates, and stabilization of the SAMs by van der Waals forces (~1 to 2 kcal mol^{-1} per methylene unit) lead to the formation of densely packed monolayers.[14,68,70,71] Prior to characterization of the SAMs, the slides were rinsed with THF followed by ethanol and dried with ultra-pure nitrogen.

A Rudolph Auto El III ellipsometer equipped with a He–Ne laser (632.8 nm) set at an incidence angle of 70° and a refractive index of 1.45, a value typical for organic thin films,[72] was used to obtain thickness measurements for the monolayer films. An average of three measurements per slide was used as the reported thickness.

X-ray photoelectron spectroscopy (XPS) was performed on a PHI 5700 X-ray photoelectron spectrometer with a monochromatic Al Kα X-ray source (1486.7 eV) incident at 90° relative to the axis of the hemispherical analyzer with a takeoff angle of 45° from the surface and a pass energy of 23.5 eV. The Au $4f_{7/2}$ peak was referenced to 84.0 eV in all the spectra.

Polarization-modulation infrared reflectance-absorption spectroscopy (PM-IRRAS) was performed using a Nicolet Nexus 670 Fourier transform equipped with a mercury–cadmium–telluride (MCT) detector and a Hinds Instrument PEM-90 photoelastic modulator. The surfaces were mounted at an incident angle of 80° for the *p*-polarized light with respect to the surface normal. The spectra were collected using 512 scans at a resolution of 2 cm^{-1}.

Contact angle data were obtained using a ramé-hart model 100 contact angle goniometer set up with a Matrix Technologies micro-Electrapette 25 to dispense probe liquids. The advancing contact angles (θ_a) and receding contact angles (θ_r) were obtained at a speed of 1 μL s^{-1}. The reported data were reproducible to ±1° and are an average of six measurements with readings being made from each side of three droplets on different locations along the slides (12 total measurements).

The contacting liquids used in the study include a variety of nonpolar, polar protic, and polar aprotic liquids: bromonaphthalene (BNP – Sigma Aldrich); decalin (DC – Acros Organics); hexadecane (HD – Aldrich); perfluorodecalin (FDC – Synquest Labs); acetonitrile (MeCN – Sigma Aldrich); nitrobenzene (NB – Acros); dimethylformamide (DMF – Sigma Aldrich); dimethyl sulfoxide (DMSO – Sigma Aldrich); formamide (FA – Sigma Aldrich); glycerol (GY – Sigma Aldrich); and water (H_2O – Millipore water with resistivity of 18.2 Ω).

Results and discussion

Ellipsometric thickness assessment

In this study, the series of CF_3-terminated SAMs were compared to their hydrocarbon analogs formed on the same batch of vapor-deposited gold that was treated electrochemically prior to formation of the SAMs. Accounts in the literature have fully characterized these hydrocarbon SAMs, which serve as a point of reference in the analysis of the SAMs on UPD Ag and the FSAMs on both substrates[36,67] Fig. 2 and Table 1 depict the average thickness measurements for the SAMs used in the study. The thickness values of the **H17SH**, **H18SH**, **H19SH**, and **H20SH** SAMs on gold exhibit thicknesses of 21, 22, 23, and 25 Å, respectively, and are in accordance with literature values.[67] Additionally, the observed increase in the thickness

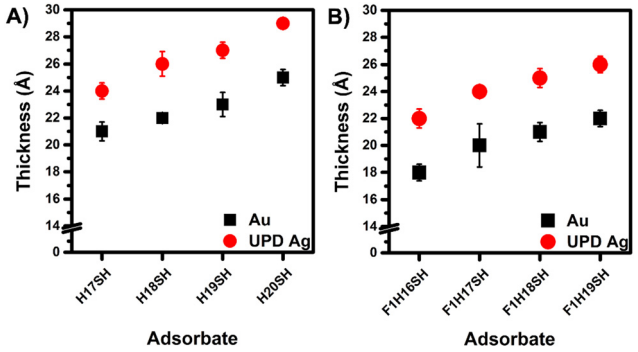

Fig. 2 Average thickness measurements obtained for the (A) **H*n*SH** SAMs and the (B) **F1H*m*SH** SAMs on Au (■) and UPD Ag (●).

Table 1 Ellipsometric thickness values of the investigated SAMs

Adsorbate	Au thickness (Å)	UPD Ag thickness (Å)	Adsorbate	Au thickness (Å)	UPD Ag thickness (Å)
H17SH	21	24	**F1H16SH**	18	22
H18SH	22	26	**F1H17SH**	20	24
H19SH	23	27	**F1H18SH**	21	25
H20SH	25	29	**F1H19SH**	22	26

values with increasing chain length, ∼1 Å, is consistent with the increase in the methylene units of the hydrocarbon backbone.[68,73] Notably, the hydrocarbon SAMs on UPD Ag are much thicker than the corresponding SAMs on Au by ∼3 Å, which is in accordance to the difference in thickness for a hydrocarbon SAM on Au and Ag in the literature.[36] Moreover, the **F1H*m*SH** analogs exhibited SAM thicknesses on gold that agree with literature values, 18, 20, 21, and 22 Å for the **F1H16SH**, **F1H17SH**, **F1H18SH**, and **F1H19SH** SAMs, respectively.[67] Following a similar trend as the **H*n*SH** SAMs, the **F1H*m*SH** adsorbates produced films that were 4 Å thicker on UPD Ag compared to their counterparts on gold.

The conformation of alkanethiols SAMs on bulk Ag have been described in the literature as having an orientation different from that of alkanethiols on Au.[13] For our study, we anticipate that the molecules on UPD Ag will behave similarly to adsorbates on bulk Ag. In terms of orientation and structure, alkanethiols on an Au surface adopt a twist angle of ∼55° and an overall tilt of ∼33°, with respect to the surface normal.[13,74,75] While on Ag surfaces, the same molecule will have a twist angle of ∼45° and a tilt of ∼10°.[13,74,75] The underlying difference in the orientation the adsorbates adopt on the metal substrates lies in the different binding geometry the sulfur atom adopts on the respective metals. Specifically, the Au–S–C bond angle is ∼104°, while the Ag–S–C bond angle is ∼180°.[76] Thus, the difference in the binding geometries dictates the orientation of the carbon backbone on the metals. Consequently, a more densely packed monolayer is formed on the UPD Ag surface as compared to the Au surfaces, a scenario that might lead to a thicker film. Given the similarities in structure between the alkanethiols and the CF_3-terminated alkanethiols (*i.e.*, the only difference is the fluorocarbon at the terminus), the CF_3-terminated alkanethiols are expected to adopt the same orientation as the former. However, we note that the CF_3-terminated alkanethiols yielded films on both gold and UPD Ag surfaces with slightly lower thickness values than the alkanethiol analogs. Previous research on CF_3-terminated alkanethiol SAMs determined the thicknesses for these types of SAMs are ∼1 Å shorter than the hydrocarbon analogs, in agreement with our observations.[67]

Analysis of the monolayer films by XPS

XPS is a surface-sensitive technique that yields qualitative and quantitative information on most elements present on a sample. In the analysis of SAMs, XPS can also give insight into the structural features of the films.[77] For the hydrocarbon SAMs, a survey scan detected the presence of Au, C and S, as well as Ag for the SAMs on UPD Ag. Fig. S3 (ESI†) shows XPS spectra of Au 4f and Ag 3d regions for the **H*n*SH** SAMs on UPD Ag surfaces. Fig. 3 and 4 depict high resolution spectra of the C 1s and S 2p regions for the hydrocarbon SAMs on Au and the Ag 3d, O 1s, C 1s, and S 2p regions for the hydrocarbon SAMs on UPD Ag, respectively. Tables S1 and S2 (ESI†) list the peak positions for the photoelectrons of the **H*n*SH** and **F1H*m*SH** SAMs on the metal substrates respectively. The high-resolution spectra for the regions of interest for the **F1H*m*SH** SAMs on Au (C 1s, F 1s, and S 2p) and UPD Ag (Ag 3d, O 1s, C 1s, F 1s, and S 2p) are shown in Fig. 5 and Fig. 6, respectively. All of the SAMs in the study, on Au and UPD Ag, exhibit a characteristic doublet with a ratio of 2 : 1 in the S 2p region, with a binding energy of ∼162.0 eV for the S $2p_{3/2}$, which is indicative of a bound thiolate.[78] Furthermore, the lack of a peak at higher binding energies, ∼164 and ∼168 eV, indicates the absence of highly oxidized sulfur species or unbound thiol on the surface. More importantly, XPS spectra of the SAMs on UPD Ag show no signals corresponding to the O 1s core level region (binding

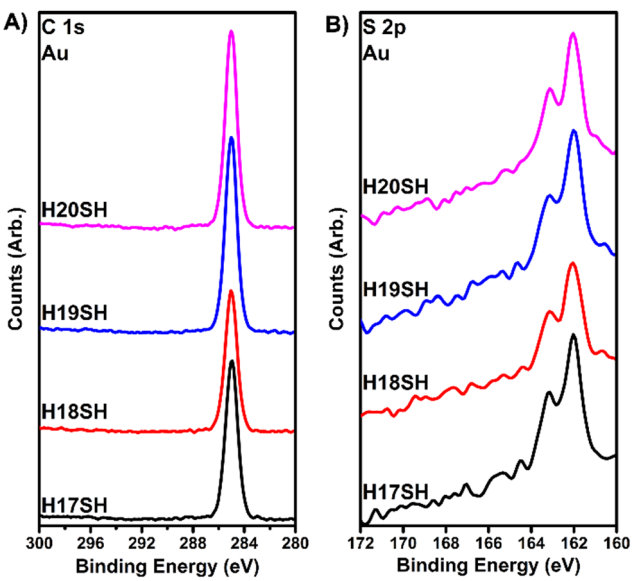

Fig. 3 XPS spectra for the (A) C 1s and (B) S 2p region for the **H*n*SH** SAMs on Au.

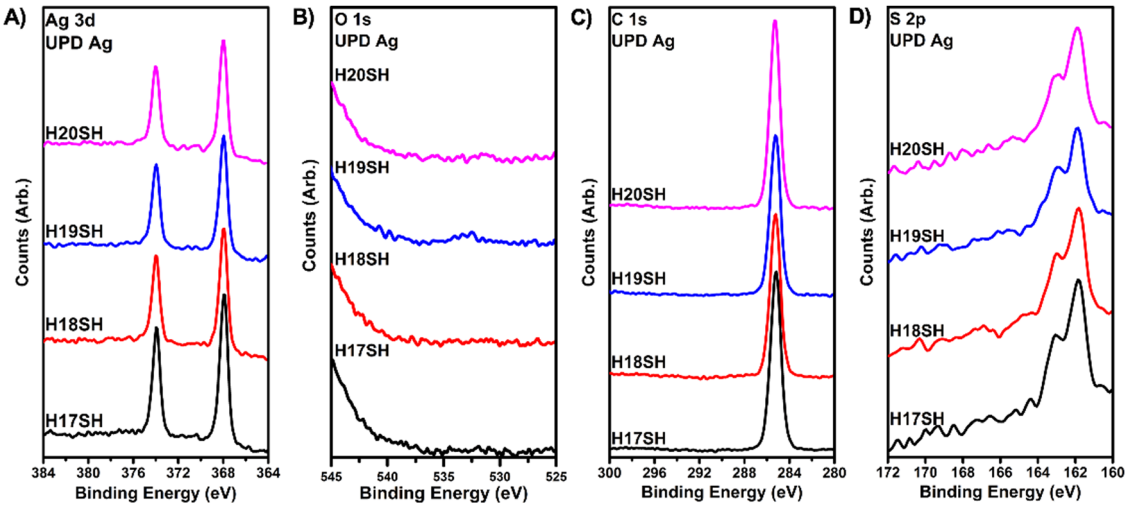

Fig. 4 XPS spectra for the (A) Ag 3d, (B) O 1s, (C) C 1s, and (D) S 2p region for the **H*n*SH** SAMs on UPD Ag.

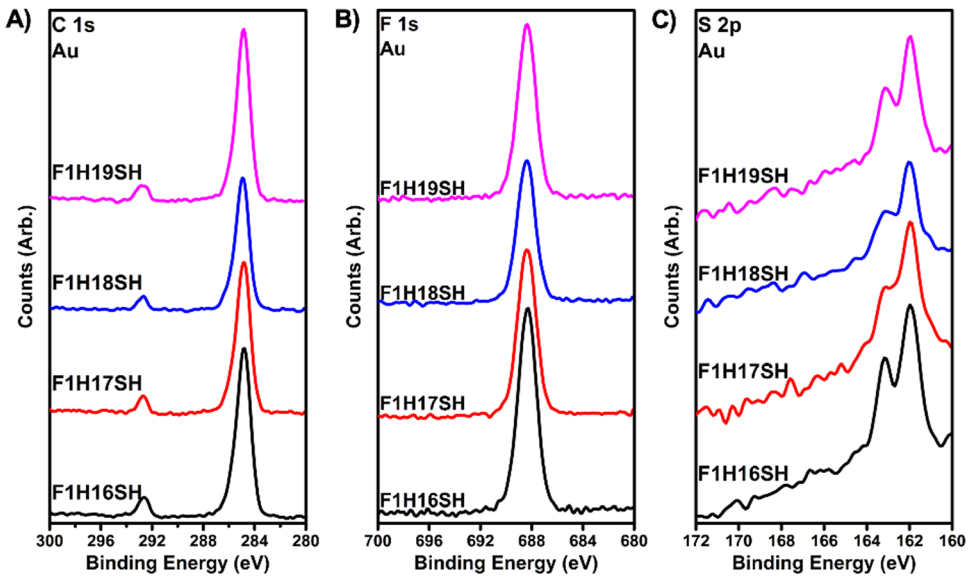

Fig. 5 XPS spectra for the (A) C 1s, (B) F 1s, and (C) S 2p region for the **F1H*m*SH** SAMs on Au.

energy ~535 eV),[77] thus confirming the absence of silver oxides. (see Fig. 4(A) and (B) as well as Fig. 6(A) and (B)).

In addition to obtaining the elemental composition and oxidation state of elements present in a SAM, a qualitative examination of the packing density of the chains can be obtained from the binding energy of the C 1s peak. For the hydrocarbon SAMs on Au, the C 1s peak appears at ~284.9 ± 0.1 eV while on UPD Ag the same peak is at ~285.2 ± 0.1 eV. The shifts to a higher binding energies for the hydrocarbon SAMs on UPD Ag are indicative of a more densely packed film compared to the comparative films on Au.[79] Specifically, in the present study, the observed increase in binding energy can be attributed to the chains being more upright on the UPD Ag surface.[80,81] On the other hand, the binding energy of C 1s for the FSAMs on Au, shows a slight decrease (~284.8 eV) in comparison to the hydrocarbon SAMs on Au, which suggests a lower chain packing in the former films plausibly due to the larger chain termini. A similar decrease in the binding energy is seen when comparing the FSAMs on UPD Ag to the hydrocarbon SAMs on UPD Ag, 285.1 eV and ~285.2 eV, respectively. However, it should be noted that between the two metal substrates, the FSAMs on UPD Ag exhibit a shift to higher binding energy for the C 1s electrons, which is in accordance with the trend observed in the hydrocarbon SAMs on the two metals. Nevertheless, the trends observed in the XPS spectra of the SAMs suggest that the methylene chains on Ag are more upright and therefore allow for a more densely packed film, as previously concluded in a friction-force microscopy study of SAMs on Au and Ag which saw increased stability in SAMs on Ag due to their greater packing density compared to the monolayers on Au.[82]

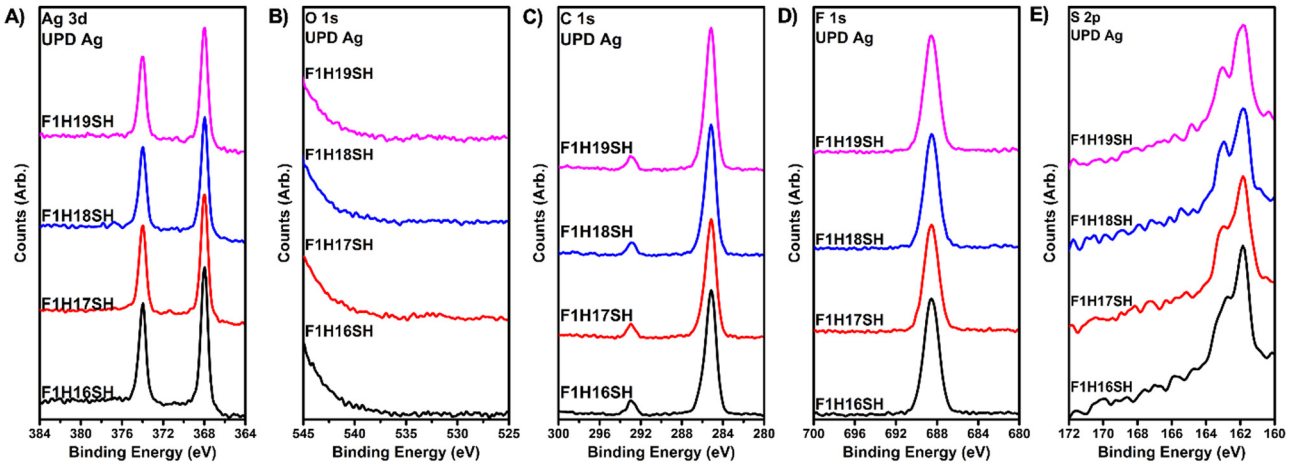

Fig. 6 XPS spectra for the (A) Ag 3d, (B) O 1s, (C) C 1s, (D) F 1s, and (E) S 2p region for the **F1H*m*SH** SAMs on UPD Ag.

Conformational order by PM-IRRAS

SAMs were characterized using PM-IRRAS to gain insight into the relative crystallinity and conformational order of the alkyl chains in the organic monolayer thin films. The conformational order of the SAMs is determined by the position of the C–H antisymmetric stretch of the methylene units $\left(\nu_{as}^{CH_2}\right)$. Appearance of this band at 2918 cm^{-1} indicates that the hydrocarbon chains are well ordered and exhibit a trans-extended conformation, making crystalline-like surfaces.[83,84] On the other hand, a shift to a higher wavenumber is characteristic of a disordered, or liquid-like film. For the hydrocarbon SAMs on Au, all of the SAMs in the series are well ordered, as shown in Fig. 7, displaying their $\nu_{as}^{CH_2}$ at 2918 cm^{-1}. A similar observation can be seen with the hydrocarbon SAMs on UPD Ag with the $\nu_{as}^{CH_2}$ at 2918/2917 cm^{-1}.

Another aspect to note from the analysis of the SAMs on both substrates from the PM-IRRAS spectra involves the difference in intensity of the methyl antisymmetric to symmetric C–H stretches, $\nu_{as}^{CH_3}$ at ~2964 cm^{-1} and $\nu_{s}^{CH_3}$ at ~2878 cm^{-1}. A discernable "odd–even" effect is observed with the ratio of the intensities of the aforementioned bands. For the SAMs on Au, the intensity of the symmetric and antisymmetric stretches on the even SAMs, **H18SH** and **H20SH**, is roughly the same, ~1 : 1 ratio. On the other hand, in the odd SAMs, **H17SH** and **H19SH**, the intensity of the symmetric C–H stretch is weaker than the intensity of the antisymmetric stretch, leading to a higher antisymmetric to symmetric stretching ratio, ~2 : 1. Interestingly, for these hydrocarbon SAMs on UPD Ag, the trends are the opposite. For the even-numbered chains, **H18SH** and **H20SH**, the intensity of the antisymmetric stretching band is higher than that of the symmetric stretching, while for the odd-numbered chains, **H17SH** and **H19SH**, the intensity of the two stretching bands is roughly the same. The reason for the change in the intensities can be attributed to the orientation of the methyl termini in the films on the two metal surfaces, as illustrated in Fig. 8. According to metal-surface selection rules governed by the PM-IRRAS technique, the intensity of vibrations whose transition dipole moments lie parallel to the surface normal are enhanced, while the intensity diminishes for vibrations with a transition dipole moment more perpendicular to the surface normal.[79] For the hydrocarbon SAMs on Au, the terminal methyl group in the odd-numbered chains is tilted away from the surface normal, giving a transition dipole moment for the symmetric stretch that is slightly perpendicular to the surface normal; whereas in the even-numbered chains, the transition dipole moment is parallel to the surface normal, and *vice versa* for the antisymmetric

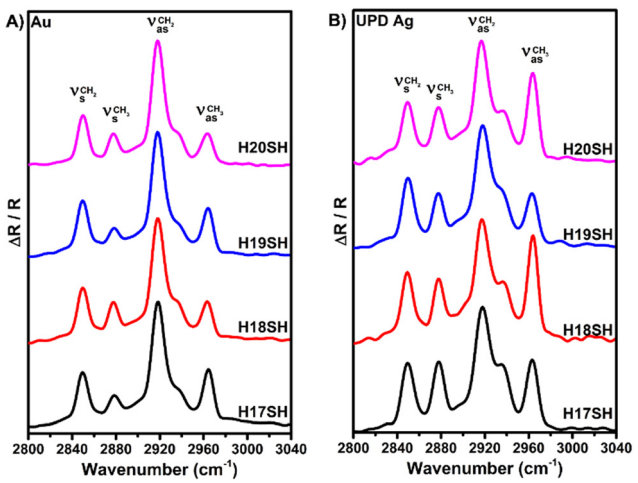

Fig. 7 PM-IRRAS spectra of the **H*n*SH** SAMs on (A) Au and (B) UPD Ag.

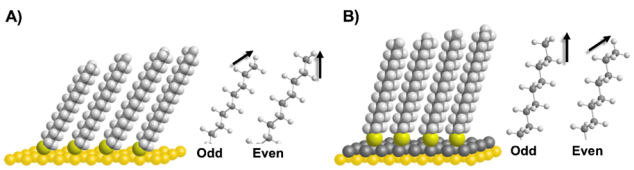

Fig. 8 Illustration of the **H*n*SH** SAMs on (A) Au and (B) UPD Ag surfaces with the orientation of the terminal methyl group for odd and even numbered chains.

stretch. However, the direction of the terminal methyl group is opposite in hydrocarbon SAMs on UPD Ag; the odd-numbered chains have a more upward orientation, while the even numbered chains have a tilted direction.

In a similar fashion, the relative ratio between the methylene antisymmetric to symmetric stretches changes depending on the substrate; the effect is apparent in the spectra of the FSAMs rather than in the spectra of the HSAMs (*vide infra*). The ratio between the methylene peaks is decidedly lower for the SAMs on UPD Ag than Au. This can also be explained according to the surface selection rule. As the chains tilt upright with respect to the surface normal, the methylene antisymmetric transition dipole moment must be getting progressively perpendicular to the surface normal, causing a lower ratio between the methylene stretching mode intensities.[76]

The PM-IRRAS spectra of the CF_3-terminated FSAMs in Fig. 9 shows that the **F1H*m*SH** SAMs on the Au and UPD Ag surfaces are well-ordered, with the alkyl chains having a *trans*-extended configuration. Previous studies on these types of FSAMs have shown that the carbon backbones have similar structural features as the hydrocarbon analogs.[85] Interesting to note in the spectra of the FSAMs, is the differences in the relative ratios of the intensities of the methylene symmetric and antisymmetric stretches between the two metal surfaces. For the FSAMs on UPD Ag, the relative ratio of the antisymmetric to symmetric stretch appears to be lower than that for the FSAMs on Au. This phenomenon might be due to either an increase in the intensity of the symmetric stretch or a decrease in the intensity of the antisymmetric stretch; both likely arise from a decrease in chain tilt on the UPD Ag surface.[86]

In contrast to the alkanethiol SAMs, the spectra of the FSAMs show a discernable "odd–even" effect in the relative ratios of the methylene stretches between odd and even chain-length molecules. The lack of odd–even effects in the C–H stretching vibrations of the methylene moieties in the **H*n*SH** SAMs suggests a uniform chain orientation on the surface for these films.[77] Previous studies on SAMs have shown that an additional degree of freedom in the terminal group can exhibit changes in the extent of the odd–even effects in relation to molecular orientation.[87–90] Alkanethiol SAMs terminated with rigid aryl groups with odd numbered chains show a higher packing density due to the upright molecular orientation compared to the inclined orientation of terminal groups in even numbered alkyl chains.[87,88] However, Dauselt *et al.* observed a diminished odd–even effect for anthracene terminated SAMs,[89] a behavior resulting from the rotation of the terminal moiety leading to greater packing of even numbered alkyl chains.[89,90] In contrast, in this study, the presence of a bulky fluorinated moiety allows the methylene units beneath it to rotate about their chain axis due to a lower packing density compared to non-fluorinated alkanes.[91] Therefore, it can be inferred that, owing to the bulkiness of the CF_3 terminus, the adjacent methylene group is likely to demonstrate a certain degree of molecular mobility, giving rise to a shift in the surface orientation of the chains.[85] An intriguing observation is the apparent reversal of the "odd–even" effect in the relative ratios of the methylene peaks when the substrate is changed from Au to UPD Ag. For the odd FSAMs (**F1H16SH** and **F1H18SH**) on Au, the relative ratio between the antisymmetric and symmetric stretches appears to be lower than the even FSAMs (**F1H17SH** and **F1H19SH**). The opposite trend is observable for the FSAMs on UPD Ag. This reversed trend suggests that the termini of the chains might be rearranging to attain a lower surface energy, leading to alterations in the intensity of the peaks.[67]

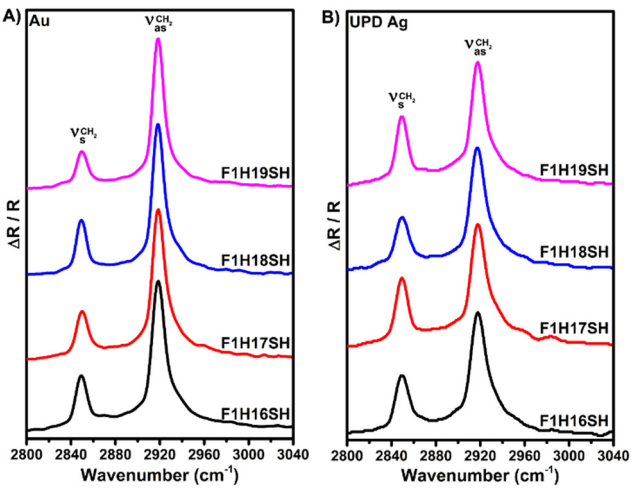

Fig. 9 PM-IRRAS spectra of the **F1H*m*SH** SAMs on (A) Au and (B) UPD Ag.

Wettability

The 'odd–even effect' is a well-known characteristic of *n*-alkanes. Physical parameters such as melting points, densities, and thermodynamic properties of fusion and sublimation of *n*-alkanes have exhibited odd–even alterations.[92,93] The molecular origin of these variations arise from the 'packing effect' where in odd-numbered alkyl chains, the terminal methyl moieties are oriented to minimize interactions with neighboring terminal groups, reducing packing efficiency and leading to lower melting points and densities compared to the more tightly packed even-numbered *n*-alkane chains.[92,93] Similarly, alkanethiol assemblies have exhibited odd–even effects in electronic properties such as current–voltage response,[94] charge transport, capacitance, chemical reactivity, and tribological properties among others.[42,75] In this study, *n*-alkanethiol SAMs on Au and UPD Ag were probed with a variety of liquids ranging in polarity to evaluate the odd–even effect on SAM wettability on the two different metals. The probe liquids used were: water – H_2O; glycerol – GL; formamide – FA; dimethyl sulfoxide – DMSO; dimethylformamide – DMF; nitrobenzene – NB; acetonitrile – ACN; bromonaphthalene – BNP; decalin – DC; hexadecane – HD; and perfluorodecalin – FDC. Surface tension values of the contacting liquids are presented in Table S3 (ESI†).[95–97]

Fig. 10 shows the advancing contact angle values for the hydrocarbon SAMs on Au and UPD Ag for the nonpolar liquids: BNP, DC, HD, and FDC. Separately, Fig. 11 shows the contact angles for the polar contacting liquids: H_2O, GL, FA, DMSO, DMF, ACN, and NB. (see also Tables S4 and S5, ESI†). For the hydrocarbon SAMs on Au, there is an odd–even effect in which

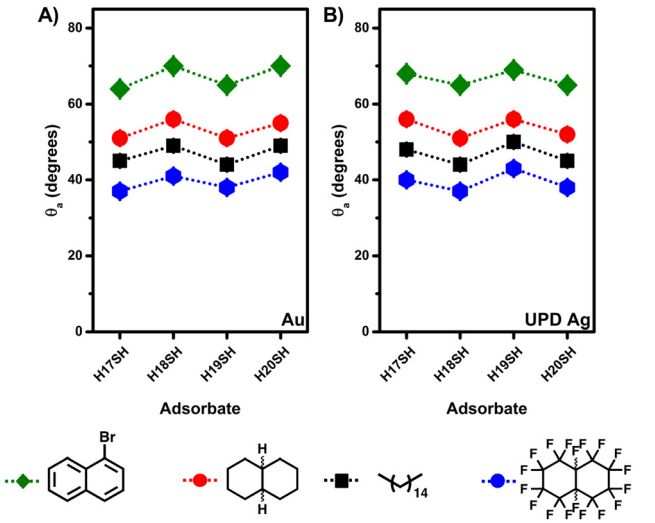

Fig. 10 Advancing contact angles for BNP, DC, HD, and FDC on **H*n*SH** SAMs on (A) Au and (B) UPD surfaces. Error bars fall within the symbols.

the odd chains (total number of carbon atoms in the chain) are more wettable than the even chains. This phenomenon can be attributed to the orientation of the terminal methyl group: in the even SAMs, the methyl group is oriented more perpendicular to the surface, while in the odd SAMs, it is tilted away (see Fig. 8) allowing for an increase in molecular contact with the underlying CH_2 unit.[98] For the hydrocarbon SAMs on UPD Ag, the odd–even effect is the opposite; the even SAMs are more wettable than the odd ones. The inversion of the odd even effect for the UPD Ag surfaces can also be attributed to the orientation of the terminal methyl group: in the odd SAMs, the methyl group is more perpendicular to the surface, while in the even SAMs, it is tilted as illustrated in Fig. 8. Moreover, the odd–even effect observed in the wettability of the hydrocarbon SAMs on both substrates is in accordance with the interpretation made above in the PM-IRRAS section for these SAMs (*vide supra*).

The advancing contact angles for nonpolar liquids on the FSAMs are presented in Fig. 12 and those of polar liquids in Fig. 13. (see also Tables S5 and S6, ESI†). With the nonpolar liquids, the contact angle values for the FSAMs are higher than those on the hydrocarbon SAMs. On the hydrocarbon SAMs, there are favorable dispersive interactions between the nonpolar liquids and the hydrocarbon surfaces. On the FSAMS, there are unfavorable non-ideal interactions between the fluorinated surface and the hydrocarbon liquids. These observations follow the phenomena of ''like dissolves like''. Moreover, the contact angles of the polar liquids are lower on the FSAMs when compared to the hydrocarbon SAMs. This observation has been attributed to the presence of an interfacial dipole in the FSAMs.[64]

The FSAMs on Au show an odd–even effect in which the even chains are more wettable than the odd ones for both sets of liquids tested. Important to note is the inversion of the odd–even effect observed for the FSAMs from what is observed with the hydrocarbon SAMs. The trends in the wettability of the hydrocarbon SAMs can be explained in terms of atomic contact between the surface and the contacting liquid.[67] However, the same argument cannot be made with the FSAMs. Previous research with CF_3-terminated alkanethiols has demonstrated that the presence of a permanent dipole at the interface of these types of SAMs has a profound effect on the wettability of the films.[62–64] For the FSAMs on Au, the dipole is oriented more along the surface normal in even chains ($\sim 17^\circ$ with respect to the surface normal) while for the odd chains it is tilted away ($\sim 58^\circ$ with respect to the surface normal).[67] When the dipoles are aligned along the surface (*i.e.*, the even chains) there are greater dipole–dipole interactions when in contact with the polar liquids, but only dipole-induced dipole interactions when in contact with the nonpolar liquids. On the other hand, when the dipoles are canted (*i.e.* the odd chains) there is a compensation between the dipoles which leads to a reduced favorable interaction between the surface and the liquid.

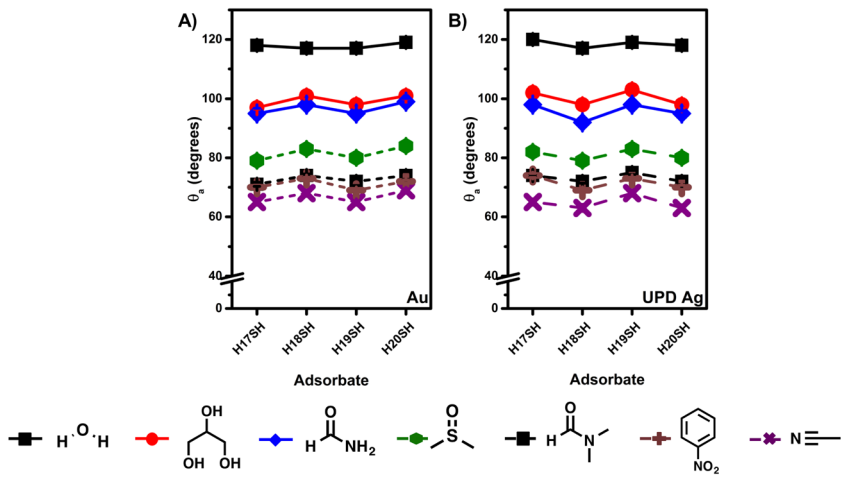

Fig. 11 Advancing contact angles for H_2O, GL, FA, DMSO, DMF, NB, and ACN on **H*n*SH** SAMs on (A) Au and (B) UPD surfaces. Error bars fall within the symbols.

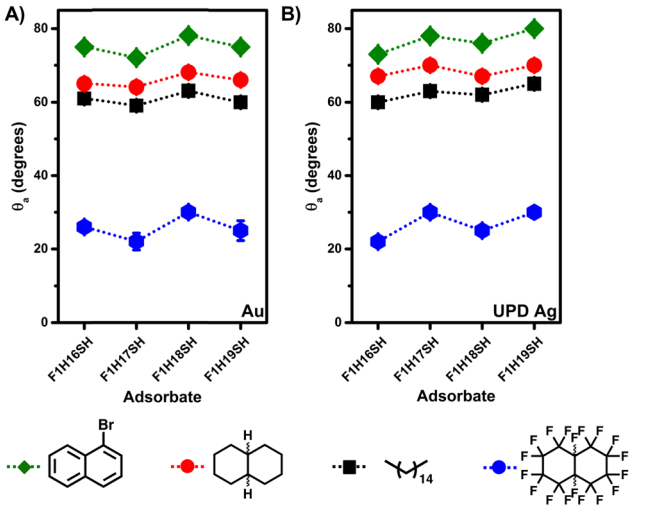

Fig. 12 Advancing contact angles for BNP, DC, HD, and FDC on **F1H*m*SH** SAMs on (A) Au and (B) UPD Ag surfaces. Error bars fall within the symbols.

In the case of FDC, the odd–even effect that is observed cannot be attributed to a dipole effect, but is more likely due to van der Waals (induced dipole-induced dipole) interactions. In the even-numbered chains, the CF_3 group is pointed more along the surface normal, exclusively exposing fluorine atoms, whereas in the odd chains, the CF_3 group is canted, exposing the underlying CH_2. Exposure of the CH_2 in the odd chains causes an unfavorable dispersive interaction with the fluorinated liquid and a higher contact angle.

For the FSAMs on UPD Ag, the odd–even effect is opposite to that observed on Au. Previous research has shown that the CF_3-terminated SAMs have similar structural properties as their hydrocarbon analogs.[85] Correspondingly, it is reasonable to assume that the CF_3-terminated alkanethiols on the UPD Ag surfaces will have similar structural properties as the alkanethiols on UPD Ag. Taking the twist and tilt angle, $\sim 45^\circ$ and $\sim 11^\circ$ respectively, that an alkanethiol adopts on a silver surface[13,75] gives the model featured in Fig. 14. It is apparent from the wettability data and the model in Fig. 14, that the CF_3 termini on the films have the opposite orientation on the silver surface.

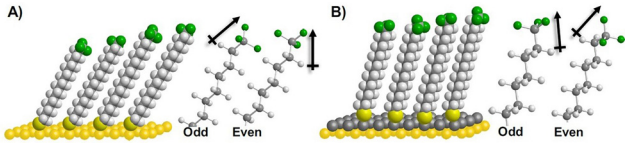

Fig. 14 Illustration of the **F1H*m*SH** SAMs on (A) Au and (B) UPD Ag surfaces with the orientation of the dipole for odd and even numbered chains.

The crystallographic structure and properties of alkanethiol SAM systems are known to differ depending on whether the molecules contain an odd or even number of carbon atoms.[99] A simulation study by Ramin *et al.* showed the relationship between carbon parity to structural characteristics of the films.[99] However, considering the number of methylene units of SAMs used in our study, results in literature showed that for molecules where $n >$ C15, structural features such as the tilt angle, tilt angle orientation, *gauche* defects and *trans* percentage has no dependence on the odd–even effect or on the chain length. These SAM structures exhibit a similarly strong and uniform structural order, confirming that the significant differences in wettability observed in this study as an 'odd–even effect' stem from the interfacial dipole induced by the orientation of the terminal moiety.

Conclusions

The alkanethiols and CF_3-terminated alkanethiols in this study were used to form SAMs on Au and UPD Ag with distinct properties. Analysis of the films by ellipsometry showed that the thickness of the SAMs on UPD Ag were thicker by ~ 4 Å than the corresponding SAMS on Au. The thicker film was attributed

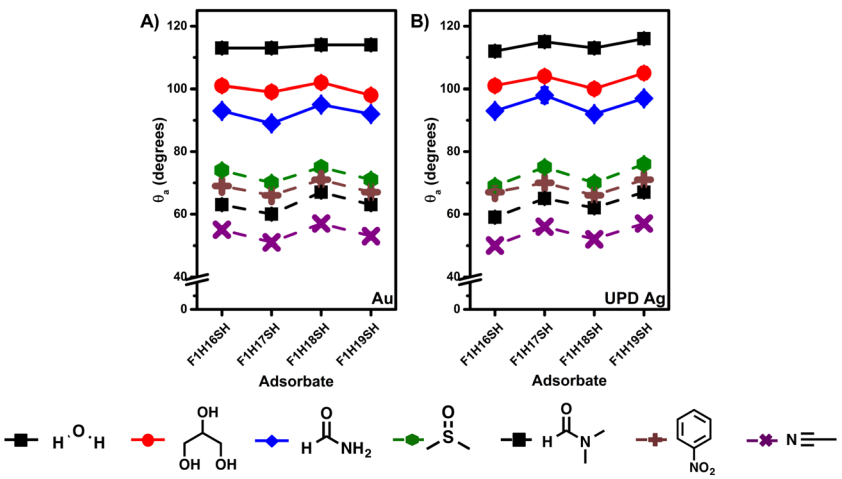

Fig. 13 Advancing contact angles for H_2O, GL, FA, DMSO, DMF, NB, and ACN on **F1H*m*SH** SAMs on (A) Au and (B) UPD surfaces. Error bars fall within the symbols.

to the inherent differences in the binding geometry of the sulfur anchor to the metal substrate, which leads to changes in tilt angles adopted by the chains. Analysis by XPS confirmed the composition of the films and presence of an unoxidized Ag layer. Further analysis revealed a more densely packed monolayer on UPD Ag than on Au. The increase in packing density of the SAMs on UPD Ag likely arises from the molecules being more upright, due to the $(\sqrt{7} \times \sqrt{7})R19^{\circ}$ adlayer structure, allowing them to pack more densely and thus contributing to the formation of thicker films. Further, analysis by PM-IRRAS revealed well-ordered films with the chains adopting a *trans*-extended conformation on both substrates. Moreover, the wettability data obtained from the SAMs generated on both substrates allowed us to probe the direction of the dipole, further highlighting the likely changes in the chain orientation between the two substrates.

Author contributions

Conceptualization: T. R. L.; formal analysis: M. M., D. R., R. A., T. R. L. and S. B.; funding acquisition: T. R. L. and S. B.; investigation: M. M., D. R., R. A., O. Z., H. J. L., T. Y. and S. S.; methodology: M. M., D. R., T. R. L. and S. B.; project administration: T. R. L. and S. B.; resources: T. R. L. and S. B.; supervision: T. R. L. and S. B.; validation: M. M., D. R., R. A., T. R. L. and S. B.; writing – original draft: M. M. and R. A.; writing – review & editing: T. R. L.

Data availability

The data supporting this article have been included as part of the ESI.†

Conflicts of interest

There are no conflicts to declare.

Acknowledgements

The authors are grateful for financial support from the NSF Division of Chemistry (CHE-2109174 and CHE-2246583).

References

1 G. V. Latag, T. Nakamura, D. Palai, E. A. Q. Mondarte and T. Hayashi, Investigation of three-dimensional bacterial adhesion manner on model organic surfaces using quartz crystal microbalance with energy dissipation monitoring, *ACS Appl. Bio. Mater.*, 2023, **6**, 1185–1194.

2 K. Son, T. Uzawa, Y. Ito, T. Kippin, K. W. Plaxco and T. Fujie, Survey of oligoethylene glycol-based self-assembled monolayers on electrochemical aptamer-based sensor in biological fluids, *Biochem. Biophys. Res. Commun.*, 2023, **668**, 1–7.

3 J. Yang, M. Zhou, J. Liu, H. Wang and C. Weng, Fabrication and tribological properties of self-assembled monolayers of alkanethiols on nickel substrates, *Appl. Surf. Sci.*, 2021, **559**, 149963.

4 O. Cooper, H.-P. Phan, B. Wang, S. Lowe, C. J. Day, N.-T. Nguyen and J. Tiralongo, Functional microarray platform with self-assembled monolayers on 3C-silicon carbide, *Langmuir*, 2020, **36**, 13181–13192.

5 L. Feng, S. Zheng, H. Zhu, X. Ma and Z. Hu, Corrosion inhibition of novel dithiane self-assembled monolayers (SAMs) on copper, *J. Taiwan Inst. Chem. Eng.*, 2023, **142**, 104610.

6 J. Telegdi, Formation of self-assembled anticorrosion films on different metals, *Materials*, 2020, **13**, 5089.

7 C. S. Park, H. J. Lee, A. C. Jamison and T. R. Lee, Robust maleimide-functionalized gold surfaces and nanoparticles generated using custom-designed bidentate adsorbates, *Langmuir*, 2016, **32**, 7306–7315.

8 H. J. Lee, A. C. Jamison, Y. Yuan, C.-H. Li, S. Rittikulsittichai, I. Rusakova and T. R. Lee, Robust carboxylic acid-terminated organic thin films and nanoparticle protectants generated from bidentate alkanethiols, *Langmuir*, 2013, **29**, 10432–10439.

9 Y. Choi, H.-V. Tran and T. R. Lee, Self-assembled monolayer coatings on gold and silica surfaces for antifouling applications: A review, *Coatings*, 2022, **12**, 1462.

10 L. R. Hill, J. W. Craft, P. Chinwangso, H.-V. Tran, M. D. Marquez and T. R. Lee, Antifouling coatings generated from unsymmetrical partially fluorinated spiroalkanedithiols, *ACS Appl. Bio. Mater.*, 2021, **4**, 1563–1572.

11 K. R. Kahsar, D. K. Schwartz and J. W. Medlin, Control of metal catalyst selectivity through specific noncovalent molecular interactions, *J. Am. Chem. Soc.*, 2014, **136**, 520–526.

12 P. D. Coan, C. A. Farberow, M. B. Griffin and J. W. Medlin, Organic modifiers promote furfuryl alcohol ring hydrogenation via surface hydrogen-bonding interactions, *ACS Catal.*, 2021, **11**, 3730–3739.

13 J. C. Love, L. A. Estroff, J. K. Kriebel, R. G. Nuzzo and G. M. Whitesides, Self-assembled monolayers of thiolates on metals as a form of nanotechnology, *Chem. Rev.*, 2005, **105**, 1103–1170.

14 C. Vericat, M. E. Vela, G. Benitez, P. Carro and R. C. Salvarezza, Self-assembled monolayers of thiols and dithiols on gold: New challenges for a well-known system, *Chem. Soc. Rev.*, 2010, **39**, 1805–1834.

15 P. N. Floriano, O. Schlieben, E. E. Doomes, I. Klein, J. Janssen, J. Hormes, E. D. Poliakoff and R. L. McCarley, A grazing incidence surface X-ray absorption fine structure (GIXAFS) study of alkanethiols adsorbed on Au, Ag, and Cu, *Chem. Phys. Lett.*, 2000, **321**, 175–181.

16 I. Martinovic, G. Zlatic, Z. Pilic, L. Susie, O. Kowalska, D. Petrovic, F. Falak and J. Miskovic, Self-assembled monolayers of alkanethiol as inhibitors against copper corrosion in synthetic acid rain, *Int. J. Electrochem. Sci.*, 2019, **14**, 4206–4215.

17 W. Zhao, M. Göthelid, S. Hosseinpour, M. B. Johansson, G. Li, C. Leygraf and C. M. Johnson, The nature of self-assembled octadecylphosphonic acid (ODPA) layers on copper substrates, *J. Colloid Interface Sci.*, 2021, **581**, 816–825.

18 P. He, A. H. S. Daaoub, S. Sangtarash, H. Sadeghi and H. J. Yoon, Thermopower in underpotential deposition-based molecular junctions, *Nano Lett.*, 2024, **24**, 1988–1995.
19 M. Hong, Y. Yokota, R. A. Wong, N. Hayazawa, E. Kazuma and Y. Kim, Underpotential deposition of silver on gold for surface catalysis of plasmon-enhanced reduction of 4-nitrothiophenol, *J. Phys. Chem. C*, 2021, **125**, 16569–16575.
20 Z. Dursun, Ş. U. Karabiberoğlu, B. Gelmez and A. Başaran, Electrocatalytic oxidation of ethanol on various metal adlayer modified Au(111) electrodes in alkaline solution, *Turk. J. Chem.*, 2011, **35**, 349–359.
21 J. W. F. Robertson, D. J. Tiani and J. E. Pemberton, Underpotential deposition of thallium, lead, and cadmium at silver electrodes modified with self-assembled monolayers of (3-mercaptopropyl)trimethoxysilane, *Langmuir*, 2007, **23**, 4651–4661.
22 P. Sebastián-Pascual and M. Escudero-Escribano, Surface characterization of copper electrocatalysts by lead underpotential deposition, *J. Electroanal. Chem.*, 2021, **896**, 115446.
23 F. W. S. Lucas, N. C. Ramos, D. K. Schwartz, J. W. Medlin and A. Holewinski, Understanding reactivity of self-assembled monolayer-coated electrodes: SAM-induced surface reconstruction, *Electrochim. Acta*, 2023, **459**, 142586.
24 M. R. Ehrenburg, E. B. Molodkina, P. Broekmann and A. V. Rudnev, Underpotential deposition of silver on Au(111) from an air- and water-stable ionic liquid visualized by in-situ STM, *ChemElectroChem*, 2019, **6**, 1149–1156.
25 I. Park and H. Baltruschat, In situ friction study of Ag underpotential deposition (UPD) on Au(111) in aqueous electrolyte, *Chem. Phys. Chem.*, 2021, **22**, 952–959.
26 M. Yang, H. Zhang and Q. Deng, Understanding the copper underpotential deposition process at strained gold surface, *Electrochem. Commun.*, 2017, **82**, 125–128.
27 Z. Tan, K. Li, Y. Gu, Z. Nan, W. Wang, L. Sun, B. Mao and J. Yan, Unconventional electrochemical behaviors of Cu underpotential deposition in a chloride-based deep eutectic solvent: High underpotential shift and low coverage, *Anal. Chem.*, 2023, **95**, 6458–6466.
28 N. Mayet, K. Servat, K. B. Kokoh and T. W. Napporn, Probing the surface of noble metals electrochemically by underpotential deposition of transition metals, *Surfaces*, 2019, **2**, 257–276.
29 E. Herrero, L. J. Buller and H. D. Abruña, Underpotential deposition at single crystal surfaces of Au, Pt, Ag and other materials, *Chem. Rev.*, 2001, **101**, 1897–1930.
30 D. M. Kolb, M. Przasnyski and H. Gerischer, Underpotential deposition of metals and work function differences, *J. Electroanal. Chem. Interfacial Electrochem.*, 1974, **54**, 25–38.
31 C. Cai, X. Ma, Y. Li, R. Zhou, C. An and J. Li, Investigation of copper underpotential deposition on polycrystalline gold electrodes, *Int. J. Electrochem. Sci.*, 2023, **18**, 100317.
32 G. A. Ragoisha, Y. M. Aniskevich, A. S. Bakavets and E. A. Streltsov, Electrochemistry of metal adlayers on metal chalcogenides, *J. Solid State Electrochem.*, 2020, **24**, 2585–2594.
33 C. Jin and I. Taniguchi, Electrocatalytic activity of silver modified gold film for glucose oxidation and its potential application to fuel cells, *Mater. Lett.*, 2007, **61**, 2365–2367.
34 A. F. Meese, C. Napier, D. J. Kim, K. Rigby, T. Hedtke, D. Leshchev, E. Stavitski, L. R. Parent and J. Kim, Underpotential deposition of 3D transition metals: Versatile electrosynthesis of single-atom catalysts on oxidized carbon supports, *Adv. Mater.*, 2024, **36**, 2311341.
35 M.-H. Hsieh and C. Chen, Scanning tunneling microscopy observations of butanethiol self-assembled monolayers on Ag underpotential deposition modified Au(111), *Langmuir*, 2000, **16**, 1729–1733.
36 G. K. Jennings and P. E. Laibinis, Self-assembled n-alkanethiolate monolayers on underpotentially deposited adlayers of silver and copper on gold, *J. Am. Chem. Soc.*, 1997, **119**, 5208–5214.
37 G. K. Jennings and P. E. Laibinis, Underpotentially deposited metal layers of silver provide enhanced stability to self-assembled alkanethiol monolayers on gold, *Langmuir*, 1996, **12**, 6173–6175.
38 S.-Y. Lin, T.-K. Tsai, C.-M. Lin, C. Chen, Y.-C. Chan and H.-W. Chen, Structures of self-assembled monolayers of n-alkanoic acids on gold surfaces modified by underpotential deposition of silver and copper: Odd−even effect, *Langmuir*, 2002, **18**, 5473–5478.
39 H. Aitchison, H. Lu, S. W. L. Hogan, H. Früchtl, I. Cebula, M. Zharnikov and M. Buck, Self-assembled monolayers of oligophenylenecarboxylic acids on silver formed at the liquid–solid interface, *Langmuir*, 2016, **32**, 9397–9409.
40 M. DeLeon and S. Baldelli, Electroreductive desorption of alkanethiols on gold and UPD copper/gold surfaces using in situ second harmonic generation, *J. Electrochem. Soc.*, 2020, **167**, 166519.
41 R. Ortiz de la Morena, A. Asyuda, H. Lu, H. Aitchison, K. Turner, S. M. Francis, M. Zharnikov and M. Buck, Shape controlled assembly of carboxylic acids: Formation of a binary monolayer by intercalation into molecular nanotunnels, *Phys. Chem. Chem. Phys.*, 2020, **22**, 4205–4215.
42 Z. Wang, J. Chen, S. Oyola-Reynoso and M. Thuo, The Porter-Whitesides discrepancy: Revisiting odd-even effects in wetting properties of n-alkanethiolate SAMs, *Coatings*, 2015, **5**, 1034–1055.
43 J. Wang, V. Gadenne, L. Patrone and J.-M. Raimundo, Self-assembled monolayers of push–pull chromophores as active layers and their applications, *Molecules*, 2024, **29**, 559.
44 H. J. Lee, A. C. Jamison and T. R. Lee, Surface dipoles: A growing body of evidence supports their impact and importance, *Acc. Chem. Res.*, 2015, **48**, 3007–3015.
45 E. Zojer, A. Terfort and M. Zharnikov, Concept of embedded dipoles as a versatile tool for surface engineering, *Acc. Chem. Res.*, 2022, **55**, 1857–1867.
46 M. Li, Y. Cao, K. Xie and J. Tang, Molecular engineering on kinetics-driven self-assembled monolayers working as auxiliary layers on dielectrics in organic field-effect transistors, *Adv. Electron. Mater.*, 2024, **10**, 2300712.
47 H. Ren, M. Ouyang, J. Wang, L. Zhang and Y. Fu, Direct self-assembled monolayers treatment on the polar polymer dielectric towards ultra-flexible organic field-effect transistors, *Mater. Lett.*, 2022, **324**, 132495.

48 W. Li, E. Martínez-Ferrero and E. Palomares, Self-assembled molecules as selective contacts for efficient and stable perovskite solar cells, *Mater. Chem. Front.*, 2024, **8**, 681–699.
49 W. Jiang, M. Liu, Y. Li, F. R. Lin and A. K.-Y. Jen, Rational molecular design of multifunctional self-assembled monolayers for efficient hole selection and buried interface passivation in inverted perovskite solar cells, *Chem. Sci.*, 2024, **15**, 2778–2785.
50 J. Koc, L. Schardt, K. Nolte, C. Beyer, T. Eckhard, P. Schwiderowski, J. L. Clarke, J. A. Finlay, A. S. Clare, M. Muhler, A. Laschewsky and A. Rosenhahn, Effect of dipole orientation in mixed, charge-equilibrated self-assembled monolayers on protein adsorption and marine biofouling, *ACS Appl. Mater. Interfaces*, 2020, **12**, 50953–50961.
51 D. Blasi, L. Sarcina, A. Tricase, A. Stefanachi, F. Leonetti, D. Alberga, G. F. Mangiatordi, K. Manoli, G. Scamarcio, R. A. Picca and L. Torsi, Enhancing the sensitivity of biotinylated surfaces by tailoring the design of the mixed self-assembled monolayer synthesis, *ACS Omega*, 2020, **5**, 16762–16771.
52 M. Singh, N. Kaur and E. Comini, The role of self-assembled monolayers in electronic devices, *J. Mater. Chem. C*, 2020, **8**, 3938–3955.
53 D. Zhang, C. Li, G. Zhang, J. Tian and Z. Liu, Phototunable and photopatternable polymer semiconductors, *Acc. Chem. Res.*, 2024, **57**, 625–635.
54 L. Wang, U. S. Schubert and S. Hoeppener, Surface chemical reactions on self-assembled silane-based monolayers, *Chem. Soc. Rev.*, 2021, **50**, 6507–6540.
55 A. Batdelger, S.-G. Lee and S.-G. Park, The effect of terminal group of hole injection self-assembled monolayers on the performance of optoelectronic devices on ITO anodes, *Mater. Chem. Phys.*, 2023, **301**, 127666.
56 E. Arkan, E. Yalcin, M. Unal, M. Z. Y. Arkan, M. Can, C. Tozlu and S. Demic, Effect of functional groups of self-assembled monolayer molecules on the performance of inverted perovskite solar cell, *Mater. Chem. Phys.*, 2020, **254**, 123435.
57 D. Rodriguez, M. D. Marquez, O. Zenasni, L. T. Han, S. Baldelli and T. R. Lee, Surface dipoles induce uniform orientation in contacting polar liquids, *Chem. Mater.*, 2020, **32**, 7832–7841.
58 C. Fischer, S. Das, Q. Zhang, Y. Liu, L. Weinhardt, D. O'Hagan, M. Zharnikov and A. Terfort, Lateral dipole moments induced by all-*cis*-pentafluorocyclohexyl groups cause unanticipated effects in self-assembled monolayers, *Nano Res.*, 2023, **16**, 11030–11041.
59 O. Zenasni, A. C. Jamison and T. R. Lee, The impact of fluorination on the structure and properties of self-assembled monolayer films, *Soft Matter*, 2013, **9**, 6356.
60 J. Li, W. Cao, J. Li and M. Ma, Fluorination to enhance superlubricity performance between self-assembled monolayer and graphite in water, *J. Colloid Interface Sci.*, 2021, **596**, 44–53.
61 C.-W. Chang, H.-H. Hsu, C.-S. Hsu and J.-T. Chen, Achieving area-selective atomic layer deposition with fluorinated self-assembled monolayers, *J. Mater. Chem. C*, 2021, **9**, 14589–14595.
62 R. Colorado and T. R. Lee, Physical organic probes of interfacial wettability reveal the importance of surface dipole effects, *J. Phys. Org. Chem.*, 2000, **13**, 796–807.
63 M. Graupe, T. Koini, H. I. Kim, N. Garg, Y. F. Miura, M. Takenaga, S. S. Perry and T. R. Lee, Wettability and friction of CF_3-terminated monolayer films on gold, *Mater. Res. Bull.*, 1999, **34**, 447–453.
64 M. Graupe, M. Takenaga, T. Koini, R. Colorado and T. R. Lee, Oriented surface dipoles strongly influence interfacial wettabilities, *J. Am. Chem. Soc.*, 1999, **121**, 3222–3223.
65 R. Colorado and T. R. Lee, Wettabilities of self-assembled monolayers on gold generated from progressively fluorinated alkanethiols, *Langmuir*, 2003, **19**, 3288–3296.
66 M. D. Marquez, O. Zenasni, D. Rodriguez, T. Yu, S. Sakunkaewkasem, F. Toro Figueira, A. Czader, S. Baldelli and T. R. Lee, Burying the inverted surface dipole: Self-assembled monolayers derived from alkyl-terminated partially fluorinated alkanethiols, *Chem. Mater.*, 2020, **32**, 953–968.
67 O. Zenasni, M. D. Marquez, A. C. Jamison, H. J. Lee, A. Czader and T. R. Lee, Inverted surface dipoles in fluorinated self-assembled monolayers, *Chem. Mater.*, 2015, **27**, 7433–7446.
68 C. D. Bain, E. B. Troughton, Y. T. Tao, J. Evall, G. M. Whitesides and R. G. Nuzzo, Formation of monolayer films by the spontaneous assembly of organic thiols from solution onto gold, *J. Am. Chem. Soc.*, 1989, **111**, 321–335.
69 M. Azhagurajan, T. Itoh and K. Itaya, Ultra-high-resolution differential interference microscopy of Ag deposition on an ultraflat Au(111), *J. Phys. Chem.*, 2016, **120**, 16221–16227.
70 L. Srisombat, A. C. Jamison and T. R. Lee, Stability: A key issue for self-assembled monolayers on gold as thin-film coatings and nanoparticle protectants, *Colloids Surf., A*, 2011, **390**, 1–19.
71 C. Vericat, M. E. Vela and R. C. Salvarezza, Self-assembled monolayers of alkanethiols on Au(111): surface structures, defects and dynamics, *Phys. Chem. Chem. Phys.*, 2005, **7**, 3258–3268.
72 M. D. Porter, T. B. Bright, D. L. Allara and C. E. D. Chidsey, Spontaneously organized molecular assemblies. 4. structural characterization of n-alkyl thiol monolayers on gold by optical ellipsometry, infrared spectroscopy, and electrochemistry, *J. Am. Chem. Soc.*, 1987, **109**, 3559–3568.
73 C. D. Bain and G. M. Whitesides, Attenuation lengths of photoelectrons in hydrocarbon films, *J. Phys. Chem.*, 1989, **93**, 1670–1673.
74 C. Du, R. S. Andino, M. C. Rotondaro, S. W. Devlin, S. Erramilli, L. D. Ziegler and M. M. Thuo, Substrate roughness and tilt angle dependence of sum-frequency generation odd–even effects in self-assembled monolayers, *J. Phys. Chem.*, 2022, **126**, 7294–7306.
75 F. Tao and S. L. Bernasek, Understanding odd−even effects in organic self-assembled monolayers, *Chem. Rev.*, 2007, **107**, 1408–1453.

76 I.-W. P. Chen, C.-C. Chen, S.-Y. Lin and C. Chen, Effect of underpotentially deposited adlayers on sulfur bonding schemes of organothiols self-assembled on polycrystalline gold: sp or sp^3 hybridization, *J. Phys. Chem. B*, 2004, **108**, 17497–17504.

77 P. E. Laibinis, G. M. Whitesides, D. L. Allara, Y. T. Tao, A. N. Parikh and R. G. Nuzzo, Comparison of the structures and wetting properties of self-assembled monolayers of n-alkanethiols on the coinage metal surfaces, copper, silver, and gold, *J. Am. Chem. Soc.*, 1991, **113**, 2370–7167.

78 D. G. Castner, K. Hinds and D. W. Grainger, X-ray photoelectron spectroscopy sulfur 2p study of organic thiol and disulfide binding interactions with gold surfaces, *Langmuir*, 1996, **12**, 5083–5086.

79 J. C. Vickerman and I. S. Gilmore, *Surface analysis: The principal techniques*, Wiley, 2009.

80 K. Heister, L. S. O. Johansson, M. Grunze and M. Zharnikov, A detailed analysis of the C 1s photoemission of n-alkanethiolate films on noble metal substrates, *Surf. Sci.*, 2003, **529**, 36–46.

81 J. Jia, A. Giglia, M. Flores, O. Grizzi, L. Pasquali and V. A. Esaulov, 1,4-Benzenedimethanethiol interaction with Au(110), Ag(111), Cu(100), and Cu(111) surfaces: Self-assembly and dissociation processes, *J. Phys. Chem. C*, 2014, **118**, 26866–26876.

82 N. J. Brewer, T. T. Foster, G. J. Leggett, M. R. Alexander and E. McAlpine, Comparative investigations of the packing and ambient stability of self-assembled monolayers of alkanethiols on gold and silver by friction force microscopy, *J. Phys. Chem. B*, 2004, **108**, 4723–4728.

83 R. A. MacPhail, H. L. Strauss, R. G. Snyder and C. A. Elliger, Carbon-hydrogen stretching modes and the structure of n-alkyl chains. 2. Long, all-trans chains, *J. Phys. Chem.*, 1984, **88**, 334–341.

84 R. G. Snyder, H. L. Strauss and C. A. Elliger, Carbon-hydrogen stretching modes and the structure of n-alkyl chains. 1. Long, disordered chains, *J. Phys. Chem.*, 1982, **86**, 5145–5150.

85 J. Pflaum, G. Bracco, F. Schreiber, R. Colorado, O. E. Shmakova, T. R. Lee, G. Scoles and A. Kahn, Structure and electronic properties of CH_3- and CF_3-terminated alkanethiol monolayers on Au(111): A scanning tunneling microscopy, surface X-ray and helium scattering study, *Surf. Sci.*, 2002, **498**, 89–104.

86 S. Frey, K. Heister, M. Zharnikov, M. Grunze, K. Tamada, R. Colorado, M. Graupe, O. E. Shmakova and T. R. Lee, Structure of self-assembled monolayers of semifluorinated alkanethiols on gold and silver substrates, *Isr. J. Chem.*, 2000, **40**, 81–97.

87 S. Lee, A. Puck, M. Graupe, R. ColoradoJr, Y.-S. Shon, T. R. Lee and S. S. Perry, Structure, wettability, and frictional properties of phenyl-terminated SAMs, *Langmuir*, 2001, **17**, 7364–7370.

88 F. Chesneau, B. Schüpbach, K. Szelągowska-Kunstman, N. Ballav, P. Cyganik, A. Terfort and M. Zharnikov, Self-assembled monolayers of perfluoroterphenyl-substituted alkanethiols: specific characteristics and odd–even effects, *Phys. Chem. Chem. Phys.*, 2010, **12**, 12123–12137.

89 J. Dauselt, J. Zhao, M. Kind, R. Binder, A. Bashir, A. Terfort and M. Zharnikov, Compensation of the odd−even effects in araliphatic self-assembled monolayers by nonsymmetric attachment of the aromatic part, *J. Phys. Chem. C*, 2011, **115**, 2841–2854.

90 W. Azzam, A. Subaihi, M. Rohwerder, A. Bashir, A. Terfort and M. Zharnikov, Odd–even effects in aryl-substituted alkanethiolate SAMs: Nonsymmetrical attachment of aryl unit and its impact on the SAM structure, *Phys. Chem. Chem. Phys.*, 2024, **26**, 7563–7572.

91 J. F. Rabolt, T. P. Russell and R. J. Twieg, Structural studies of semifluorinated n-alkanes. 1. Synthesis and characterization of $F(CF_2)_n(CH_2)_mH$ in the solid state, *Macromolecules*, 1984, **17**, 2786–2794.

92 J. C. S. Costa, A. Mendes and L. M. N. B. F. Santos, Chain length dependence of the thermodynamic properties of n-alkanes and their monosubstituted derivatives, *J. Chem. Eng. Data*, 2018, **63**, 1–20.

93 K. Yang, Z. Cai, A. Jaiswal, M. Tyagi, J. S. Moore and Y. Zhang, Dynamic odd–even effect in liquid n-alkanes near their melting points, *Angew. Chem., Int. Ed.*, 2016, **55**, 14090–14095.

94 H. Cabrera-Tinoco, A. C. L. Moreira, R. Valencia-Bedregal, L. Borja-Castro, A. Perez-Carreño, A. Lalupu-García, C. Mendoza-Alejo, C. H. W. Barnes, J. W. Seo and L. D. L. S. Valladares, Effective coupling model to treat the odd−even effect on the current−voltage response of saturated linear carbon chains single-molecule junctions, *ACS Omega*, 2024, **9**, 35323–35331.

95 F. M. Fowkes, F. L. Riddle, W. E. Pastore and A. A. Weber, Interfacial interactions between self-associated polar liquids and squalane used to test equations for solid---liquid interfacial interactions, *Colloids Surf.*, 1990, **43**, 367–387.

96 I. Mc. N. Smallwood, *Handbook of organic solvent properties*, Arnold, 1996.

97 B. Jańczuk and T. Białłopiotrowicz, Surface free-energy components of liquids and low energy solids and contact angles, *J. Colloid Interface Sci.*, 1989, **127**, 189–204.

98 D. Barriet, P. Chinwangso and T. R. Lee, Can cyclopropyl-terminated self-assembled monolayers on gold be used to mimic the surface of polyethylene?, *ACS Appl. Mater. Interfaces*, 2010, **2**, 1254–1265.

99 L. Ramin and A. Jabbarzadeh, Odd–even effects on the structure, stability, and phase transition of alkanethiol self-assembled monolayers, *Langmuir*, 2011, **27**, 9748–9759.